

Mathematical Modeling and Numerical Analysis of the Programming Field in PEO₁₀LiCF₃SO₃-Polypyrrole Neural Switch

MAHMOUD Z. ISKANDARANI

Faculty of Science and Information Technology

Al-Zaytoonah Private University of Jordan

P.O.BOX 911597, Post Code: 11191

JORDAN

m_iskandarani@yahoo.com

Abstract: - The design and numerical modeling using Finite Element Analysis (FEA) of electric field strength in a programmable neural switch is carried out. The obtained model provided good approximation to the derived complex analytical solution, which is carried out by means of complex mathematical analysis employing SCHWARZ-CHRISTOFFEL transform. Effect of electrode separation and field spread in both x and y directions are studied and explained. Boundary effects on field strength representation is discussed and numerically reduced through increasing the number of nodes for each element in the finite grid. Edge effect on field strength is also eliminated using semi-infinite coplanar electrode approximation. Such a switch will function as a synaptic processor behaving in an adaptive manner and suitable to be used as a compact programmable device with other artificial neural network hardware.

Key-Words: - Neural, Numerical, Finite Element, Mathematical, Memory, Information Processing, Polymers

1 Introduction

A practical neural network would have to use data structures with modeled neurons having distributions of synapses over reasonable dendritic geometries, with spines and microcircuits, and ionic channels representation. Charge would propagate through the dendrites and soma. Action potentials would be initiated accordingly in the initial segment and would reach the terminals according to a distribution of propagation times. Other than diffusion losses, charge would remain in the soma and would be able to initiate a series of action potentials interior. The mentioned can be represented by a finite-element or multilevel adaptive approximation that approximate the appropriate electro diffusion equations [6-9].

The architecture of the brain can be viewed with greater or less granularity. Although understanding of lower-level processing is relevant to higher levels, it is possible to begin understanding the higher levels without a complete picture of the lower ones. At the level of single neurons, the several ion species present are assumed to obey a set of partial differential equations. Such equations can be numerically modeled using Finite Element Analysis, which proved to be a good approximation to the complex analytical solution and a fast tool for validation of the analytical model and future variations [1,2]. In this paper the electrostatic potential and field strength, which is an essential requirement for the operation of the neural switch is

numerically modeled using various types of finite elements. Assuming two semi-infinite co-planar electrodes separated by a gap [20].

Effect of electrode separation and distance from the origin on the field strength and device are analyzed. Mathematical representation of FEA is illustrated and discussed [21,22].

2 Background

The implementation of a neural prosthesis involves replacing a portion of the nervous system with an artificial device. Aside from developing hardware and providing for its physical and physiological integration with the nervous system, this requires logical development which comprises the following:

- (1) Abstract model that shows what computations need to be done, independently of implementation.
- (2) Theory of how these computations are implemented in real neurons.
- (3) Technology for implementing them in an artificial computer.
- (4) Plan for logical integration of the neural and the electronic computations so that they jointly have the desired effect.

For the simpler recognition and motion planning tasks, these issues can be solved by ad hoc methods; but for more complex tasks involving the integration

of multiple inputs and outputs a more systematic approach is needed.

Our picture of the neuron is that of a processing element that performs a spatio-temporal integration of incoming signals. This integration is coded in a state. The question is not so much whether a presynaptic event is sufficient to cause an action potential; rather, by changing the state it changes the ability to respond to subsequent events and it thereby modulates the dynamics of streams of action potentials. The neuron transforms streams of states in presynaptic neurons into streams of states in postsynaptic neurons, and modifies them according to its state and according to its connectivity. Also, any local stream in a neuron corresponds to the set of presynaptic streams that can bring it about, and the structure of these sets can be analyzed logically.

3 Modeling the Neural Switch

Figure 1 illustrates the designed and modeled neural switch, using Polyethylene Oxide - Lithium Trifluoromethane Sulphonate ($\text{PEO}_{10}\text{LiCF}_3\text{SO}_3$), which is known as material for high energy, long life, flexible, and re-chargeable just like a neural switch and has good mechanical and stable electrochemical properties [3-5]. The material is used together with a highly conducting polymer, called Polypyrrole (PPY) that possess excellent chemical and thermal stability and has ability to switch between two states, namely conducting (oxidized) and insulating (reduced), similar to the real neuron. Combining these polymers produced an ionic-electronic interacting mixed conductor. The resulting device was tested and proved to be able to store the injected charge, affecting its conduction and switches states due to device resistance change. Such a change would be stable occupying a specified level until another charge is injected or removed.

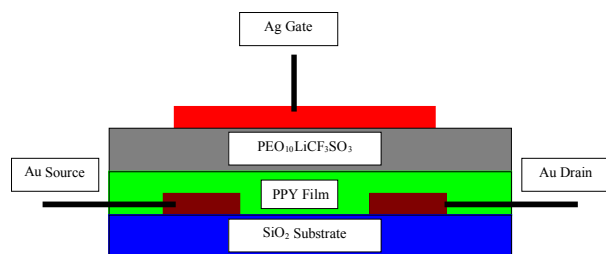


Fig. 1: Neural Switch Structure

4 Mathematical Modeling

For any regular complex potential function; its real and imaginary parts form orthogonal families of curves that satisfy the CAUCHY-RIEMANN equations, and as conjugate functions of complex variables; the real and imaginary parts of the complex potential functions also satisfy the LAPLACIAN differential equation as harmonic functions [17-18].

The orthogonality of the families of curves forming the complex potential function derived for a particular geometry can be preserved using a comprehensive and powerful mathematical theory known as the theory of CONFORMAL TRANSFORMATION. By this theory, the geometry of the complex Z-plane is mapped onto the complex potential plane, the W-plane, by means of an analytical function $w=f(z)$ which is obtained through the elimination of a third complex variable $t = u + jv$ between $z = f_1(t) = x + jy$ and $w = f_2(t) = \Phi + j\psi$. Consequently the field strength expression is then obtained as the gradient of the potential.

$f_1(t)$ and $f_2(t)$ are obtained using the SCHWARZ-CHRISTOFFEL differential equation which assumes the potential and field boundaries to be straight-line segments forming a polygon as they meet at a vertex closing up the polygonal boundary with a vertex angle.

Regarding the Z-plane as a rectilinear polygon with only few sides the SCHWARZ-CHRISTOFFEL differential equation is used twice over to connect the real axis in the t-plane with the boundary of the polygon in the Z- and W- planes in such a way that the upper-half of the t-plane transforms into the interior of the polygon.

Figure 2 shows a cross section of the two planar electrodes in the neural switch. The two co-planar electrodes in the z-plane correspond to two divergent sides of a polygon extending at infinity with a negative vertex angle and six vertices I, J, K and L, M, N. But since I, J and L, M reach infinity with an angle of $-\pi$, and K and N are symmetrical about the y-axis, then the polygonal boundary can be considered to form a three vertices polygon, namely L, M and N; with K and N having interior angles of 2π with respects to the x-axis as shown in Figure 3. A conformal transformation of the real axis of the t-plane, (Figure 4), into the interior of the polygon, (Figure 3) is carried out. Let the vertex M in the Z-plane correspond with the limit as $t \rightarrow \infty$ and assume the following correspondence between the remaining points and vertices:

(a) At N, $t = +1, z = +d, \theta_1 = 2\pi$

- (b) At $-N$, $t = -1$, $z = -d$, $\theta_2 = 2\pi$
- (c) At L , $t = 0$, $z = \infty$, $\theta_3 = -\pi$

Substitution of these points in the SCHWARZ-CHRISTOFFEL differential equation given by:

$$\frac{dz}{dt} = C_1 (t-t_1) \left(\frac{\theta_1}{\pi}\right)^{-1} (t-t_2) \left(\frac{\theta_2}{\pi}\right)^{-1} \dots (t-t_n) \left(\frac{\theta_n}{\pi}\right)^{-1} \quad (1)$$

Gives:

$$\frac{dz}{dt} = C_1 (t^2 - 1) t^{-2} = C_1 (1 - t^{-2}) \quad (2)$$

Integrating (2) yields:

$$z = F_1(t) = \int dz = C_1 \int (1 - t^{-2}) dt = C_1 \left(t + \frac{1}{t} \right) + K_1 \quad (3)$$

Where, constants C_1 and K_1 depend on the correspondence between the points in the two planes. Now applying boundary conditions (a) and (b) and solving for z will produce:

$$z = \frac{d}{2} \left(t + \frac{1}{t} \right) \quad (4)$$

The expression in equation (4) has a pole at $t = 0$, which corresponds to the infinite side of the coplanar electrodes and satisfies boundary condition (c) for $z = \infty$ at $t = 0$.

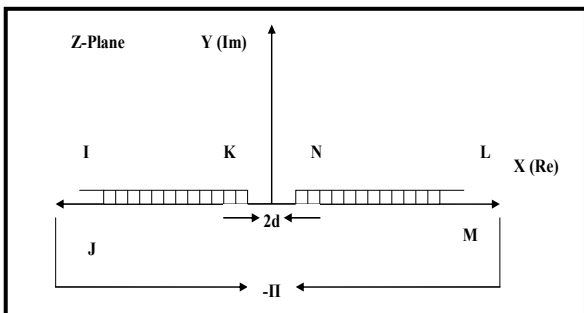


Fig2: Coplanar Electrodes Cross Section

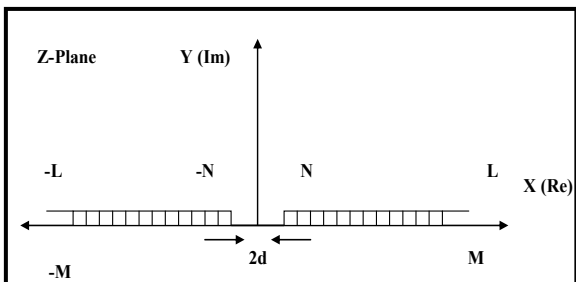


Fig 3: Z-Plane Geometrical Mapping

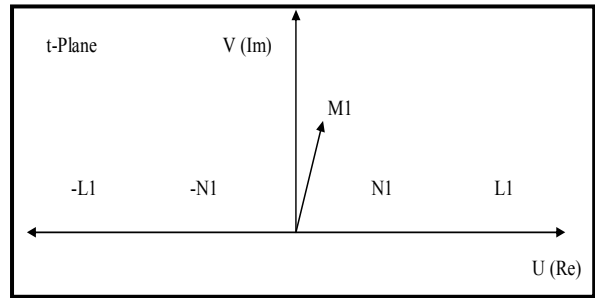


Fig 4: t-Plane Mathematical Mapping

To obtain the required field expression, (Electrical Transformation), the co-planar electrode on the positive x -axis in the z -plane is rotated by an angle π (anti clockwise) so the two semi-infinite co-planar electrodes will be transformed to two infinite parallel lines which are used in the W -plane to form a polygon as shown in Figure 5.

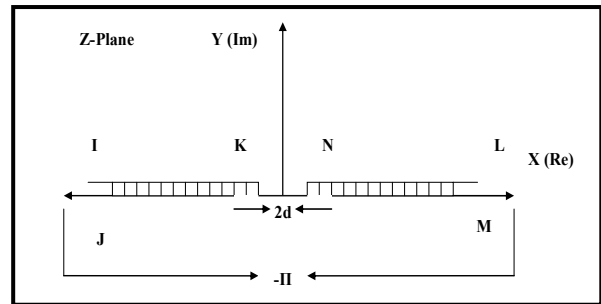


Fig.5 Electrical Transformation into W-Plane

By this rotation the vertices will meet at infinity with a vertex angle of zero, and the boundary conditions become as follows:

- (a) At $w = \infty + jV_0$, $t = -\infty$
- (b) At $w = \infty$, $t = \infty$
- (c) At $w = -\infty$, $t = 0$, $\phi = 0$

These boundary conditions describe a polygon with a single vertex. Now applying the following equation:

$$\frac{dw}{dt} = C_2 (t-t_a) \left(\frac{\phi_1}{\pi}\right)^{-1} (t-t_b) \left(\frac{\phi_2}{\pi}\right)^{-1} \dots (t-t_n) \left(\frac{\phi_n}{\pi}\right)^{-1} \quad (5)$$

Gives:

$$\frac{dw}{dt} = C_2 t^{-1} \quad (6)$$

Integration of equation (6) gives:

$$w = F_2(t) = \int dw = C_2 \int t^{-1} dt = C_2 \ln(t) + K_2 \quad (7)$$

Since points $w = -\infty$ and $t = 0$ are made to correspond, then $K_2 = 0$, then equation 7 becomes:

$$w = C_2 \ln(t) \quad (8)$$

Now, as the semi-infinite co-planar electrode on the positive x-axis is rotated by an angle π to produce the two parallel lines in the w-plane; a semi-circular arc is formed in the t-plane with radius R with the following points corresponding to each other:

- (1) At $w = \phi_0$, $t = R \exp(j0) = R$
- (2) At $w = \phi_0 + jV_0$, $t = R \exp(j\pi)$

Substituting these points in equation (8) and solving for C_2 and w yields:

$$w = \frac{V_0}{\pi} \ln(t) \quad (9)$$

Expression (9) is only defined for $t > 0$ and it has a zero at $t = 1$ and satisfies the boundary condition (c) at $t = 0$.

To obtain the complete conformal transformation, the variable t needs to be eliminated as follows:

$$t = \exp\left(\frac{\pi w}{V_0}\right) \quad (10)$$

Substituting (10) into (4) gives:

$$z = d \left[\frac{\exp(\pi w/V_0) + \exp(-\pi w/V_0)}{2} \right] = d \cosh\left(\frac{\pi w}{V_0}\right) \quad (11)$$

Hence, the complete transformation is:

$$w = \frac{V_0}{\pi} \cosh^{-1}\left(\frac{z}{d}\right) \quad (12)$$

The field strength expression is given as the gradient of the potential, so:

$$|\underline{E}| = E = \left| \frac{dw}{dz} \right| = \left| \frac{d}{dz} \left(\frac{V_0}{\pi} \cosh^{-1}\left(\frac{z}{d}\right) \right) \right| \quad (13)$$

$$= \left| \frac{V_0}{\pi(z^2 - d^2)^{1/2}} \right|$$

5 Numerical Modeling

5.1 Four-Node Plane Isoparametric Element

Let the field quantity be $\beta = \beta(x,y) = \beta(u,v)$, where u and v are dimensionless cartesian co-ordinates used to generate elements in the (x,y) plane. If an element has side lengths of $2a$ and $2b$ then u and v are given by:

$$u = \frac{x}{a}, v = \frac{y}{b} \quad (14)$$

For a four-node element, β is interpolated from nodal values $\{\beta_e\} = [\beta_1, \beta_2, \beta_3, \beta_4]^T$,

$$\beta = [N] \beta_e \text{ or } \beta = \sum_{i=1}^4 N_i \beta_i \quad (15)$$

Where N_i is the interpolation or shape function given by:

$$N_1 = \frac{1}{4}(1-u)(1-v), N_2 = \frac{1}{4}(1+u)(1-v) \quad (16)$$

$$N_3 = \frac{1}{4}(1+u)(1+v), N_4 = \frac{1}{4}(1-u)(1+v) \quad (17)$$

Where $u = \pm 1, v = \pm 1$

For an isoparametric element:

$$\begin{Bmatrix} \beta, x \\ \beta, y \end{Bmatrix} = [B] \{\beta_e\} \quad (18)$$

Where $[B]$ is given by:

$$\begin{bmatrix} N_1, x, N_2, x, N_3, x, N_4, x \\ N_1, y, N_2, y, N_3, y, N_4, y \end{bmatrix} \quad (19)$$

(19) is the displacement matrix where, x and y are given by:

$$x = \sum_{i=1}^4 N_i X_i, y = \sum_{i=1}^4 N_i Y_i \quad (20)$$

The element characteristic matrix $[K]$, with material property \mathbf{q} and element thickness t is given by:

$$[K] = \int \int [B]^T q [B] t dx dy \tag{21}$$

$$= \int_{-1}^1 \int_{-1}^1 [B]^T q [B] t J du dv$$

Where; J is the Jacobian of the transformation from u-v plane to x-y plane.

In equation (21) second form, [B] is a function of u and v and β is expressed in terms of u and v so equation (18) is re-written as:

$$\begin{Bmatrix} \beta, u \\ \beta, v \end{Bmatrix} = [D_N] \{\beta_e\} \tag{22}$$

Where,

$$[D_N] = \begin{bmatrix} N_1, u & N_2, u & N_3, u & N_4, u \\ N_1, v & N_2, v & N_3, v & N_4, v \end{bmatrix} \tag{23}$$

From equation (15):

$$N_1, u = -\frac{1}{4}(1-v), \quad N_1, v = -\frac{1}{4}(1-u) \tag{24}$$

And so on.

The relationship between (β,u), (β,v) and (β,x), (β,y) is given by:

$$\begin{Bmatrix} \beta, x \\ \beta, y \end{Bmatrix} = [J]^{-1} \begin{Bmatrix} \beta, u \\ \beta, v \end{Bmatrix} = [\Gamma] \begin{Bmatrix} \beta, u \\ \beta, v \end{Bmatrix} \tag{25}$$

From equations (18), (22) and (25) we obtain:

$$[B][\beta_e] = [\Gamma][D_N][\beta_e] \tag{26}$$

From (26):

$$[B] = [\Gamma][D_N] \tag{27}$$

Where;

$$\Gamma_{11} = u, x, \Gamma_{12} = v, x, \Gamma_{21} = u, y, \Gamma_{22} = v, y \tag{28}$$

So, the required JACOBIAN matrix [J] is given by:

$$[J] = \begin{bmatrix} x, u & y, u \\ x, v & y, v \end{bmatrix} = \begin{bmatrix} \sum_{i=1}^4 N_i, ux_i & \sum_{i=1}^4 N_i, uy_i \\ \sum_{i=1}^4 N_i, vx_i & \sum_{i=1}^4 N_i, vy_i \end{bmatrix} \tag{29}$$

$$= [D_N] \begin{bmatrix} x_1 & y_1 \\ x_2 & y_2 \\ x_3 & y_3 \\ x_4 & y_4 \end{bmatrix} \tag{30}$$

Where; D_N is given by:

$$[D_N] = \frac{1}{4} \begin{bmatrix} -(1-v)(1-v)(1+v) - (1+v) \\ -(1-u) - (1+u)(1+u)(1-u) \end{bmatrix} \tag{31}$$

From equations (28) and (29), Γ can be written as:

$$[\Gamma] = [J]^{-1} = \frac{1}{\infty} \begin{bmatrix} J_{22} & -J_{12} \\ -J_{21} & J_{11} \end{bmatrix} \tag{32}$$

Where; ∞ = det [J] = (J₁₁ J₂₂ - J₂₁ J₁₂)

The JACOBIAN is a function of u and v and it is regarded as a scale factor that transforms the area dx dy in the first form of (21) from du dv in the second form of (21).

Now all the necessary expressions are developed and by substituting them into equation (21) the characteristic matrix of a four-node quadrilateral element is evaluated using GAUSS QUADRATURE formula.

5.2 Eight-node plane isoparametric element

By placing an extra node on each side of the four-node quadrilateral element described previously a quadratic quadrilateral element is produced. As with the four-node bilinear element, the sides of the quadratic element are at u = + 1 and v = + 1. Axes u and v may be curved in the quadratic element like the ones used in the analysis.

The complete set of shape functions is as shown in equations 33 to 40:

$$N_1 = \frac{1}{4}(1-u)(1-v) - \frac{1}{2}(N_8 + N_5) \tag{33}$$

$$N_2 = \frac{1}{4}(1+u)(1-v) - \frac{1}{2}(N_5 + N_6) \tag{34}$$

$$N_3 = \frac{1}{4}(1+u)(1+v) - \frac{1}{2}(N_6 + N_7) \tag{35}$$

$$N_4 = \frac{1}{4}(1-u)(1+v) - \frac{1}{2}(N_7 + N_8) \tag{36}$$

$$N_5 = \frac{1}{2}(1-u^2)(1-v) \quad (37)$$

$$N_6 = \frac{1}{2}(1+u)(1-v^2) \quad (38)$$

$$N_7 = \frac{1}{2}(1-u^2)(1+v) \quad (39)$$

$$N_8 = \frac{1}{2}(1-u)(1-v^2) \quad (40)$$

To determine the characteristic matrix, the same procedures are followed as before. It is important to realize that isoparametric elements are geometrically isotropic, so, the numerical values of coefficients in [K] do not depend on the order of numbering of nodes. However, the order must be maintained and must run counter clockwise if J is not to become negative over part or the entire element [10-13].

6 Experimental Arrangements

In the process of planning the overall switch pattern, considerable efforts were made to allow for the following:

- (1) Uncomplicated and practical electrochemical growth and deposition of polymeric material (poly(pyrrole)), by making the size of the contact pads of the device large enough compared to the working electrode potential connections.
- (2) Elimination of the edge effect, in the Z-direction, on the conduction behavior of the device, by permitting sufficient electrode length at either side of the polymer window.
- (3) Simplification of the bonding task through formation of relatively strong bonds by deposition of NiCr on the contact pads.

6.1 Polymers Preparation

6.1.1 Poly(pyrrole)

Poly(pyrrole) films [19] were grown electrochemically using a three electrode cell consisting of:

- (1) Working electrode (finite gold electrode structure).
- (2) Reference electrode (calomel electrode).
- (3) Counter electrode (platinum gauze).

Before initiating the growth process of poly(pyrrole), nitrogen was bubbled for 20 minutes, through the working solution of 50 mmol dm⁻³

pyrrole dissolved into 0.1 mol dm⁻³ TSA (sodium salt) as the supporting electrolyte. This degassing process was carried out in order to remove any oxygen. Nitrogen was continuously passed over the surface of the solution during the growth operation to prevent re-oxygenation.

Films were grown by applying a potential step of 800 mV across the reference electrode and working electrode, while submerging the finite electrode structure in the growth solution. Current flowing between the working electrode and the counter electrode was measured over a specified period of time. As film thickness is known to be proportional to the length of time for which the potential is applied, they were grown for 60 seconds. This growth technique has the advantage of being able to produce thin films of poly(pyrrole) with an average thickness of 3.5 μm.

6.1.2 PEO₁₀LiCF₃SO₃

Polymer films [3-5] were prepared using poly(ethylene oxide) with average molecular weight of 5 x 10⁶ Daltons (Da). and density of 1.21 at 65°C, and lithium trifluoromethane sulfonate 97% pure. The required amounts of lithium salt and polyethylene oxide (PEO), to give an O:Li ratio of 10:1, were dissolved in acetonitrile 99% pure under nitrogen atmosphere. The solution was then stirred at room temperature for 48 hours after which the solution was filtered to remove any un-dissolved materials, and stored in 14, 2 ml plastic containers and kept well isolated from the atmosphere.

The polymeric films were deposited using a drop coating technique and then dried by heating for 30 minutes in an oven at 50 °C.

3. Neural Switch Programming

The RNS is programmed by means of charge storage process, which proceeds as follows:

- (1) The source and drain are shorted together.
- (2) A biasing potential is applied between the shorted terminals and the gate.
- (3) After a specific time (5 minutes) the bias voltage is removed and the source and drain disconnected from each other.
- (4) The change in the device resistance is measured as the gate is left floating.

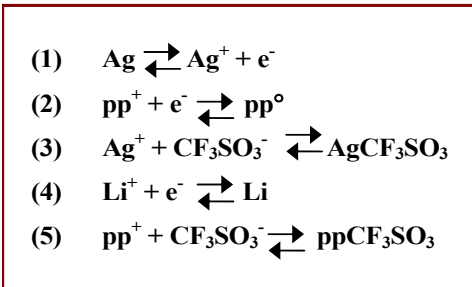
The above process was carried out over a range of positive and negative biasing potentials with the temperature kept constant at 25 °C using heating element under normal room atmosphere. The heating element was used not only to stabilize temperature at a certain value, but also to help testing the device at various temperatures. The typical programming cycle consisted of applying 0 volts up to +60 mV, and then back from +60 mV

down to 0, then immediately after that a negative cycle started by applying 0 mV to -60 mV and back from -60 mV to 0.

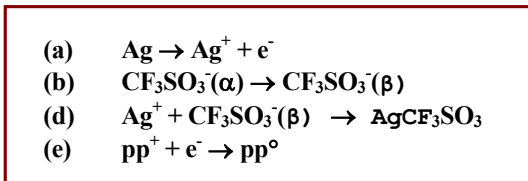
7 Discussion and Conclusion

When programmed, the bias applied between the gate and the shorted source/drain terminal will set up a field that will oxidize or reduce the polymer, as shown in the following expressions [14-16]:

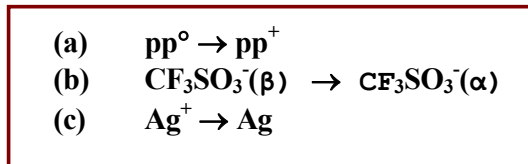
1. Gate Interactions



2. Positive Cycle



3. Negative Cycle



Hence when the programming voltage is removed and a constant current is applied between the source and drain, the measured conductance will be related to the previously applied bias and will be fixed until another latching potential is introduced. Such bias in figure 6 with expected hysteresis shown in figures 7 and 8.

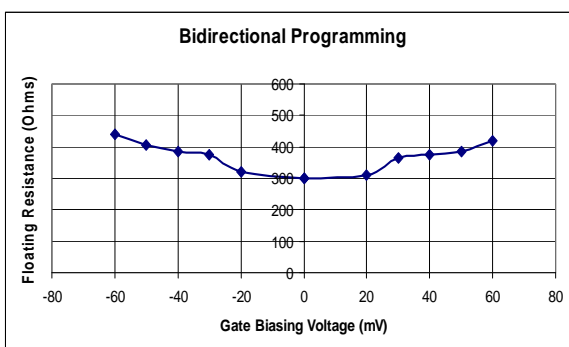


Fig 6: Gate Bidirectional bias

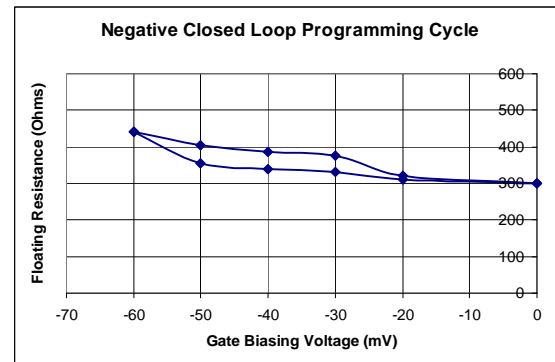


Fig 7: Negative Bias Showing Hysteresis

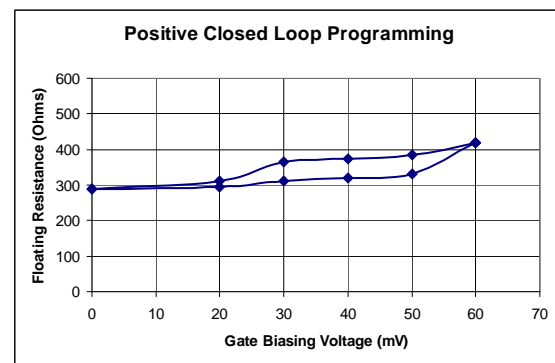


Fig 7: Positive Bias Showing Hysteresis

Such actions are related to the established electric field within the switching device where a slow and gradual (power) decrease in the programming field value is realized (figure 9) as we travel along the x-axis. This is consistent with all field theories and with the geometrical co-planar electrode construction shown in figure 2.

Also, a peak point occurred at $x=5\mu m$, which corresponds to the internal edge of the electrode structure as it equals half the separation between the electrodes ($2d = 10\mu m$) according to figure 2. Such a peak point is valid as the field strength at the inner edge is at its peak, while the one at the far edge is at its lowest. This is in agreement with the semi-infinite co-planar electrode assumption. A decrease in the field value as we travel up the y-axis (figure 10) is evident. This is also consistent with field theory and the increment of distance away from the field lines linking the device structure.

Further analysis lead to the following conclusions regarding the modeled field strength:

- (1) As the separation between the electrodes increases, the field value decreases as shown in figure 11.

- (2) The decrement in the field value as a function of distance along the y-axis is gradual and has a slow, power like characteristics, where no peak point is present as the plot considers the effect of travel along the y-axis as shown in figure 12.
- (3) Increasing the nodes per modeling element in the finite mesh resulted in more uniform field strength and better representation of the derived analytical solution, as field approximation and numerical simulation is affected by the total number of nodes used in constructing the grid needed for analysis. Figure 13 illustrates the reduction in simulation error as a function of used nodes.

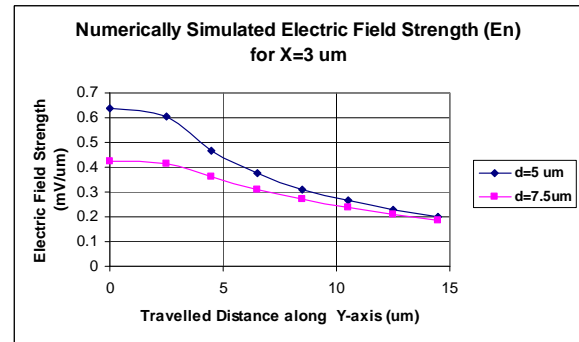


Fig. 12: Effect of Electrode Separation on the Programming Field of Neural Switch

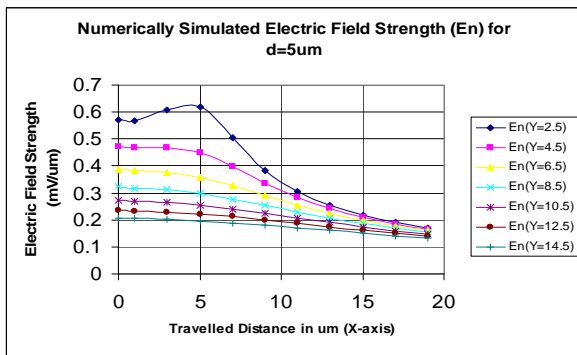


Fig. 9: Field Characteristics for Neural Switch

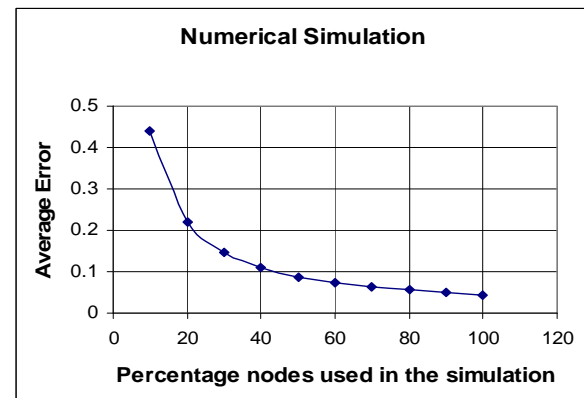


Fig. 13: Effect of Number of Nodes on modeling Accuracy

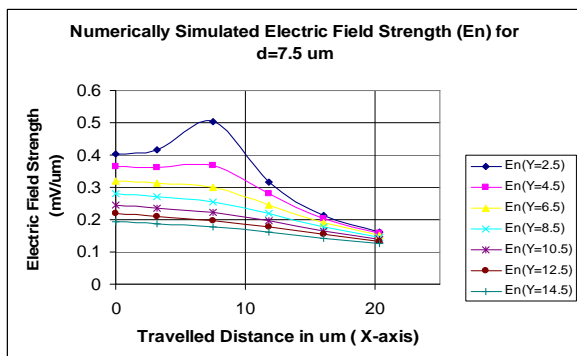


Fig. 10: Field Characteristics for Neural Switch

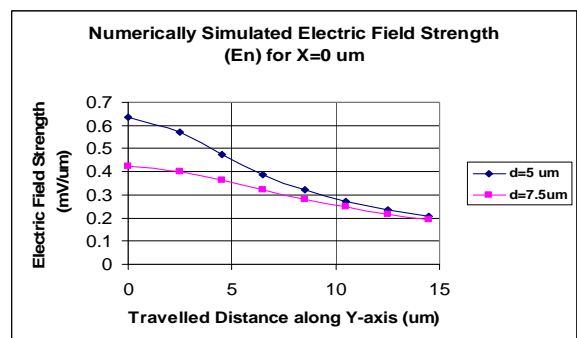


Fig. 11: Effect of Electrode Separation on the Programming Field of Neural Switch

In conclusion, a bi-directional neural switch (synapse) is successfully designed, modeled and tested with good characteristics. The design of such an artificial device can help in future implementations and studies in the fields of memories, neural networks, intelligent computers and medical applications to name a few. The device uses organic materials and depends on ionic-electronic interaction, which might not be the fastest in comparison to other types of materials and ways of carrier transport. In addition, hysteresis, which is thought to occur due to charge storage, contributed to the observed level shifting and slowness in response. However, as it is usually the case in determining range of values to which a corresponding logical action is considered, we can safely ignore hysteresis and charge storage effects if the switching speed is considered to be sufficient for a particular application. The RNS design and implementation provides a good insight into the process of combining high charge storage materials to provide intelligent switching elements. Such a switch may be used to control and modulate the communication between different artificial neurons.

References:

- [1] Misha I Rabinovich, R D Pinto, Henry D I Abarbanel, Evren Tumer, Gregg Stiesberg, R Huerta and Allen I Selverston, "Recovery of hidden information through synaptic dynamics", *Network: Comput. Neural Syst.* Vol.13, 2002 pp.487-501.
- [2] Y. Karklin, M. S. Lewicki, "A hierarchical Bayesian model for learning non-linear statistical regularities in non-stationary natural signals", *Neural Computation*, Vol.17, No.2, 2005, pp.397-423.
- [3] Anne-Vale'rie G. Ruzette, a Philip P. Soo, Donald R. Sadoway, and Anne M. Mayesz, "Melt-Formable Block Copolymer Electrolytes for Lithium Rechargeable Batteries", *Journal of The Electrochemical Society*, Vol.148, 2001, pp. A537-A543 .
- [4] S. C. Mui, a, P. E. Trapa, B. Huang, P. P. Soo, M. I. Lozow, T. C. Wang, R. E. Cohen, b A. N. Mansour, S. Mukerjee, d, A. M. Mayes, D. R. Sadoway, z, "Block Copolymer-Templated Nanocomposite Electrodes for Rechargeable Lithium Batteries", *Journal of The Electrochemical Society*, Vol.149, No.12, 2002, A1610-A1615.
- [5] Yosslen Aray, Manuel Marquez, Jesus Rodri'guez, David Vega, Yamil Simo'n-Manso, Santiago Coll, Carlos Gonzalez, David A. Weitz, "Electrostatics for Exploring the Nature of the Hydrogen Bonding in Polyethylene Oxide Hydration", *J. Phys. Chem. B*, Vol.108, 2004, pp.2418-2424.
- [6] R. Segev, Y. Shapira, M. Benvenisto, E. Ben-Jacob, "Observations and modeling of synchronized bursting in two dimensional neural networks," *Phys. Rev. E*, Vol. 64, 2001, pp 1-9.
- [7] Buitengeweg, J.R., Rutten, W.L., Marani, E. "Modeled channel distributions explain extracellular recordings from culture neurons sealed to microelectrodes," *IEEE Trans Biomed Eng.*, Vol.49, 2002, pp.1580-1590.
- [8] M. A. Corner, J. van Pelt, P. S. Wolters, R. E. Baker, and R. Nuytinck, "Physiological effects of sustained blockade of excitatory synaptic transmission on spontaneously active developing neuronal networks - an inquiry into the reciprocal linkage between intrinsic biorhythms and neuroplasticity in early ontogeny ", *Neurosci. Biobehav. Rev.*, Vol.26, 2002, pp. 127-185.
- [9] J. van Pelt, P. S. Wolters, W. L. C. Rutten, M. A. Corner, P. van Hulten, G. J. A. Ramakers, "Spatio-temporal firing in growing networks cultured on multi-electrode arrays", *Proc. World Congr. Neuroinformatics*, Rattay F (Ed) Argesim Report no. 20, Argesim/Asim Vienna, 2001, pp. 462-467.
- [10] Kaihsu Tai, Stephen D. Bond, Hugh R. MacMillan, Nathan, Andrew Baker, Michael Jay Holst, J. Andrew McCammon, " Finite Element Simulations of Acetylcholine Diffusion in Neuromuscular Junctions", *Biophysical Journal*, Vol. 84, 2003, pp.2234-2241
- [11] Volker Scheuss, Erwin Neher, "Estimating Synaptic Parameters from Mean, Variance, and Covariance in Trains of Synaptic Responses", *Biophysical Journal*, Vol.81, 2001, pp.1970-1989.
- [12] Kevin M. Franks, Thomas M. Bartol, Jr., Terrence J. Sejnowski, "A Monte Carlo Model Reveals Independent Signaling at Central Glutamatergic Synapses", *Biophysical Journal*, Vol.83, 2002, pp.2333-2348
- [13] Serdar Kuyucak, Matthew Hoyles, Shin-Ho Chung, "Analytical Solutions of Poisson's Equation for Realistic Geometrical Shapes of Membrane Ion Channels", *Biophysical Journal*, Vol.74, 1998, pp.22-36.
- [14] Mahmoud Iskandarani, " Mathematical Modeling of the Programing Field in a Neural Switch using the Semi-Infinite Coplanar Electrode Approximation ", *Advances in Complex Systems*, Vol.9, No.3, 2006, pp.193-207.
- [15] Mahmoud Iskandarani, " Design, Modeling, and Implementation of a Re-Programmable Neural Switch (RNS), *Neural Network World Journal*, Vol.16, No.3, 2006, pp.227-238.
- [16] Mahmoud Iskandarani, "Characterization of Ag-PEO₁₀LICF₃SO₃-PolyPyrrole-Au Neural Switch", *WSEAS Transactions on Computers*, Vol.8, No.7, 2008, pp.1109-2750.
- [17] J. W. Brown, R. V. Churchill, " Complex Variables and Applications", 7th edition, McGraw-Hill, 2004.
- [18] Ian Stewart, David Tall, " Complex Analysis", Cambridge University Press, 2002.
- [19] C.M. Li, C.Q. Sun, W. Chen, L. Pan, "Electrochemical thin film deposition of polypyrrole on different substrates", *Surface & Coatings Technology*, Vol.198, 2005, pp.474-477.
- [20] D. Naceur , H. Bougherira, Z. Assad, A. Guessoum, " A MOEMS architecture for a bionic retina", *Proceedings of the 7th WSEAS Int. Conf. on Signal Processing, Computational Geometry & Artificial Vision*, Athens, Greece, August 24-26, 2007, pp.241-245.

- [21]A. García-Beltrán¹, J. L. Ocaña And C. L. Molpeceres," TEMPLUM: A Process Adapted Numerical Simulation Code for The 3D Predictive Assessment of Laser Surface Heat Treatments in Planar Geometry", Wseas Transactions On Computers, Vol.7, No.2, 2008, pp.65-74.
- [22]Wang Xinwu," Nonlinear Finite Element Analysis on the Steel Frame with Semi-rigid Connections", 7th Wseas Int. Conf. On Applied Computer & Applied Computational Science (ACACOS '08), Hangzhou, China, April 6-8, 2008, pp.31-35.